AJNR

Anatomic applications of xenon-enhanced CT scanning: visual image analysis and brain-blood partition coefficient studies in man.

B P Drayer, A Friedman, D Osborne, R Albright and M Bates

Anatomic Applications of Xenon-Enhanced CT Scanning: Visual Image Analysis and Brain-Blood Partition Coefficient Studies in Man

Burton P. Drayer,[1] Allan Friedman,[2] Dennis Osborne,[1] Robert Albright,[3] and Milton Bates[1]

The inhalation of nonradioactive xenon, an inert gas that diffuses freely across the blood-brain barrier, resulted in brain enhancement which was quantitated and visualized by computed tomography (CT). Serial CT scans obtained during the buildup and equilibrium phase of xenon inhalation were used in a numerical and visual analysis of xenon accumulation in multiple selected gray- and white-matter regions in 12 patients. The calculated brain-blood partition coefficient (λ) in normal gray matter was 0.92 ± 0.11 and in normal white matter, 1.38 ± 0.14. Asymmetries and delays in xenon enhancement were often visually apparent. The estimated partition coefficient was diminished more with cerebral infarction, intracerebral hematoma, and vasogenic edema than with hypoxic encephalopathy or glioblastoma multiforme. An increase in the rate of xenon accumulation was apparent by visual inspection of the motor cortex contralateral to complex hand movements. Technical factors and potential difficulties in conducting xenon-enhanced CT studies are discussed.

Nonradioactive (stable) xenon has an atomic number and k-edge that permits its visualization and quantitation by computed tomography (CT). When the arterial blood and brain concentrations of xenon are measured by CT, a reasonably accurate assessment of regional cerebral blood flow and brain-blood partition coefficient (λ) can be made in vivo with a high degree of anatomic specificity. Studies in both nonhuman primates and man have been performed to estimate regional cerebral blood flow and λ by this method [1-7].

A practical limitation in human studies involving regional cerebral blood flow calculations is the need to monitor arterial input function. The end-tidal xenon measurement method, as popularized by Obrist et al. [8] for xenon-133, can circumvent the necessity for arterial puncture but requires a very sensitive stable xenon monitor (e.g., mass spectrometer) to obtain truly accurate input function data. Some have suggested that a thermoconductivity analyzer be used [5], but we have not found this to be sufficiently accurate. At present we use a mass spectrometer and semiclosed inhalation system, which provides accurate and reproducible absolute values for regional cerebral blood flow but requires additional personnel, temperamental and expensive equipment, and extensive computer postprocessing. These factors limit the potential usefulness of xenon-enhanced CT for routine clinical purposes. This study analyzes the straightforward human application of xenon-enhanced CT using only a standard visual image analysis and the trivial calculation of λ from the brain concentration of xenon at equilibrium.

Subjects and Methods

Subjects were 12 patients (age range, 10-49 years). Informed consent as approved by the Human Use Committee of Duke University was obtained. An intravenous line was always placed in an arm vein before studies were performed. An anesthesiologist was in attendance.

Xenon Inhalation

The subject first underwent denitrogenation by inhaling 100% oxygen for about 15 min. This also enabled the subject to become accustomed to the mouthpiece and to breathing through the ventilatory apparatus at a steady rate without moving the head. A closed anesthesia rebreathing circuit was used so less xenon would be required. About 5 L of 100% xenon was placed in a breathing bag in the closed system. Inhalation was continued for up to 10 min with the slow (100 ml/min) introduction of oxygen into the system. At 4–5 min the end-tidal xenon concentration usually begins to decrease gradually. A small amount of xenon is then bled into the closed system to maintain a stable equilibrium concentration of xenon. A calibrated thermoconductivity analyzer (Gow-Mac; Bound Brook, NJ, and Kent, England) attached by tubing to the subject's expiratory output was used to monitor the end-tidal xenon concentration. Because of the slow response time and other inaccuracies of the thermoconductivity analyzer, we were unable to get an accurate or reproducible end-tidal xenon measurement. We are now obtaining accurate end-tidal xenon information from a mass spectrometer (which was not used in these 12 subjects). The thermoconductivity analyzer was however quite useful for determining the end-tidal xenon concentration at equilibrium and could thus be used to calculate the brain-blood partition coefficient (λ).

CT Scanning

A baseline CT scan was obtained at the one or two levels of interest. Four to seven additional scans were then obtained at each chosen level during xenon inhalation at various intervals 1.5–10 min after commencement of xenon inhalation. Attempts were made to prevent even slight head movement during the scan sequence. The General Electric 8800 (5 mm collimation, 500 mA, 120 kVp, 9.6 sec scan time) and the Siemens Somatom (4 mm collimation, 460 mA, 125 kVp, 10 sec scan time) scanners were used.

Visual Analysis

The baseline scans were compared with subsequent serial scans obtained during xenon inhalation for gray matter, white matter, and lesion enhancement. Images were evaluated on the basis of improved versus decreased visualization of the pathologic abnormality. Visual inspection was also used to select the anatomic regions of interest to calculate the gray- or white-matter λ.

Quantitative Analysis

Calculations were performed from data obtained during xenon inhalation (buildup phase). The brain-blood partition coefficient (λ) for a given tissue compartment (i) can be calculated in two ways, both predicated on the experimentally confirmed concept that the estimated concentration of xenon in arterial blood and end-tidal gas are in close agreement and linear in terms of Hounsfield and thermoconductivity units.

In the first method [1–3], a direct ratio between the brain and arterial blood (or end-tidal xenon concentration × a conversion factor to CT units) concentrations when both have equilibrated will represent the λ:

$$\lambda_i = \frac{CT \# \text{ brain (at equil)} - CT \# \text{ brain (baseline)}}{CT \# \text{ blood (at equil)} - CT \# \text{ blood (baseline)}}.$$

This works quite easily for calculating the gray-matter λ (gray matter equilibrates in about 5 min), but necessitates extrapolation to equilibrium when estimating the white-matter or pathologic tissue λ. The white matter may require 20–30 min of continued xenon inhalation to equilibrate. Since the arterial and venous concentrations of xenon are almost the same at 5 min, a plastic syringe filled with venous blood and immediately placed in the CT scanner may also be used to calculate the λ and confirm the accuracy of the end-tidal xenon concentration measurements.

The second method for estimating λ_i was developed by Kelcz et al. [6]. Their working equation is:

$$CT \# \text{ blood (at equil)} = \frac{2.575 \times \theta Xe \times CXe}{UpW/UpXe \times 100},$$

where θXe equals $0.0011 \times \text{Hct}(\%) + 0.10$; CXe is the equilibrium concentration of xenon (%) as measured by the calibrated thermoconductivity analyzer; and UpW/UpXe is experimentally derived by CT scanning of blood samples with different known xenon or iodine concentrations. In this manner a pixel-by-pixel map of λ was obtained without blood samples. The regional cerebral blood flow was not calculated in these 12 patients because of inconsistent arterial input function data derived from the thermoconductivity analyzer. We did however analyze the changes (mean, standard deviation) in the brain concentration of xenon occurring over time in multiple brain regions of interest and compared these values with those in the homologous regions in the contralateral hemisphere.

Results

The CT study with inhalation levels of 30%–45% xenon was well tolerated by all subjects. Most subjects reported feeling numbness, giddiness, or a "very pleasant high," while one subject felt uncomfortable, agitated, and anxious. Head movement was not a major problem, although changes in position of 1–2 mm were sometimes seen. One subject exhibited more movement on the later scans because of laughter, and in some other subjects a larger change in position occurred on a single scan from the series.

Estimates of λ were derived for multiple anatomic sites in each subject. In addition, the degree of enhancement permitted a visual evaluation of brain anatomy and pathology.

Normal Controls (n = 3) and Motor Activation (n = 1)

A visual presentation of the progressive enhancement that occurs during xenon inhalation is shown in figure 1. The rapid increase in density in gray-matter structures (caudate, globus pallidum, putamen, thalamus, and cortical gray) as compared with white matter (internal capsule, centrum semiovale) is apparent. If inhalation were continued for 20–30 min, the white matter (λ = 1.38 ± 0.14) would become denser than the gray (λ = 0.92 ± 0.11). Asymmetric enhancement was never observed. Preferential xenon enhancement in the gray matter on the initial CT scans (first 2–5 min of inhalation) produced a striking improvement in the ability to visually distinguish gray from white matter. All regions of deep and cortical gray matter achieved greater than 95% equilibrium within 5 min as determined by unchanging gray-matter (CT regions of interest in multiple gray-matter sites) and blood (venous or end-tidal xenon) concentrations. Even with 8–10 min of xenon inhalation, the centrum semiovale, corpus callosum, and internal capsule did not reach equilibrium.

When the subject performed a complex, nonrepetitive motor task with his right hand, greater initial xenon enhancement was noted by both visual and numerical analysis in the left motor cortex region as compared with the homologous cortex on the right. As expected, within 6 min the enhancement was symmetric in both hemispheres as the brain-blood λ in both anatomic regions equilibrated.

Chronic Cerebral Infarction, Adult (n = 2)

The area of infarction increases only minimally in density as compared with uninvolved gray or white matter. The infarction was highlighted when enhancement of the adjacent uninvolved gray matter was maximal (equilibration phase). The xenon study improved visualization of subtle regions of infarction that could not be seen or were poorly visualized on the unenhanced or intravenously enhanced CT study. A meaningful λ could not be calculated from the area of infarction because of the extremely low flow, which would have necessitated a prolonged period of xenon inhalation to achieve or even extrapolate to equilibrium.

Acute Intracerebral Hematoma and Resolution (n = 1)

The xenon study did not improve visualization of the intracerebral hematoma (fig. 2). Nevertheless, by both visual and numerical analysis an area of brain adjacent to the hematoma increased in density faster than other brain regions consistent with a relative increase in flow. On a xenon CT study performed 6 weeks later, two areas of decreased enhancement representing devitalized brain were prominently seen on the equilibrium scan (10 min of inhalation) but dubiously visualized in retrospect on the baseline unenhanced image at the same level.

Sickle Cell Disease (n = 3)

In one subject without a focal neurologic deficit but with a seizure disorder, a xenon-enhanced CT study was performed to determine whether transfusion therapy should be instituted. The xenon CT study was completely normal in terms of both visual analysis and the steady progression and sequence of increasing brain concentration (fig. 3). On early scans the gray matter enhanced to a greater degree than the white matter, consistent with faster gray flow and highlighting the gray-white boundaries. By 10 min, the white matter showed greater enhancement than the gray because of its higher λ. In two other subjects with the same disorder, xenon enhancement in uninvolved brain highlighted multiple small infarctions that were not as well visualized without xenon inhalation enhancement (fig. 4).
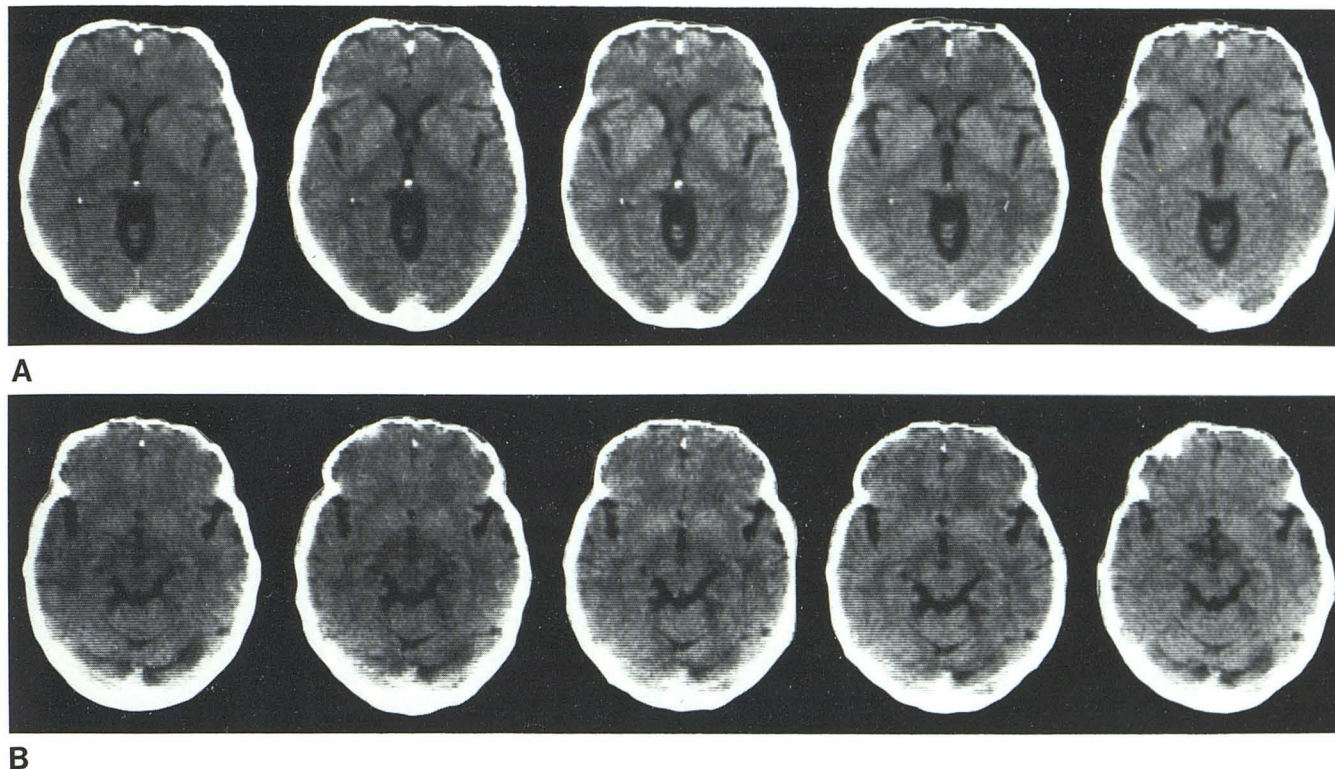
A

B

Fig. 1.—Normal CT with 31% xenon inhalation in control subject. **A**, At internal capsule level. *Left to right*: baseline scan before xenon inhalation; at 1 min 50 sec; 3 min 5 sec; 5 min 50 sec; and 8 min 35 sec after onset of inhalation. **B**, At midbrain level. *Left to right*: baseline scan before xenon inhalation; at 1 min 15 sec; 2 min 35 sec; 5 min; and 6 min 55 sec after onset of inhalation. In both series, gradual increase in gray-matter enhancement until last scan. In last scan of each series, gray matter has achieved equilibrium while white matter continues to show increasing enhancement.

Fig. 2.—Abnormal CT with 38% xenon inhalation in patient with large intracerebral hematoma and associated ventricular displacement. *Left to right*: baseline scan before xenon inhalation; at 2 min; 4 min; and 8 min after onset of inhalation. Hematoma remains unchanged in density while tissue adjacent to hematoma (*arrows*) enhances more rapidly than other areas of brain, consistent with increased flow to this region.

Chronic Hypoxic Encephalopathy with Coma Secondary to Trauma (n = 1)

Visual inspection of the xenon CT study in this chronically intubated patient revealed bilaterally symmetric enhancement of gray and white matter. Although it required a prolonged inhalation time (8 min) to achieve gray matter 95% equilibrium in selected regions of interest, the calculated λ in both gray- and white-matter sites was within the lower limits of our defined normal range.

Glioblastoma Multiforme (Post–Radiation Therapy) with Vasogenic Edema (n = 1)

Movement occurred in the subject after 5.5 min of xenon inhalation. A normal enhancement pattern was evident in the contralateral hemisphere (fig. 5). The delay in enhancement of the extensive associated vasogenic edema was more severe than in the thalamic region, which was infiltrated with neoplasm. From this single study, parameters could not be determined to distinguish infiltrating neo-
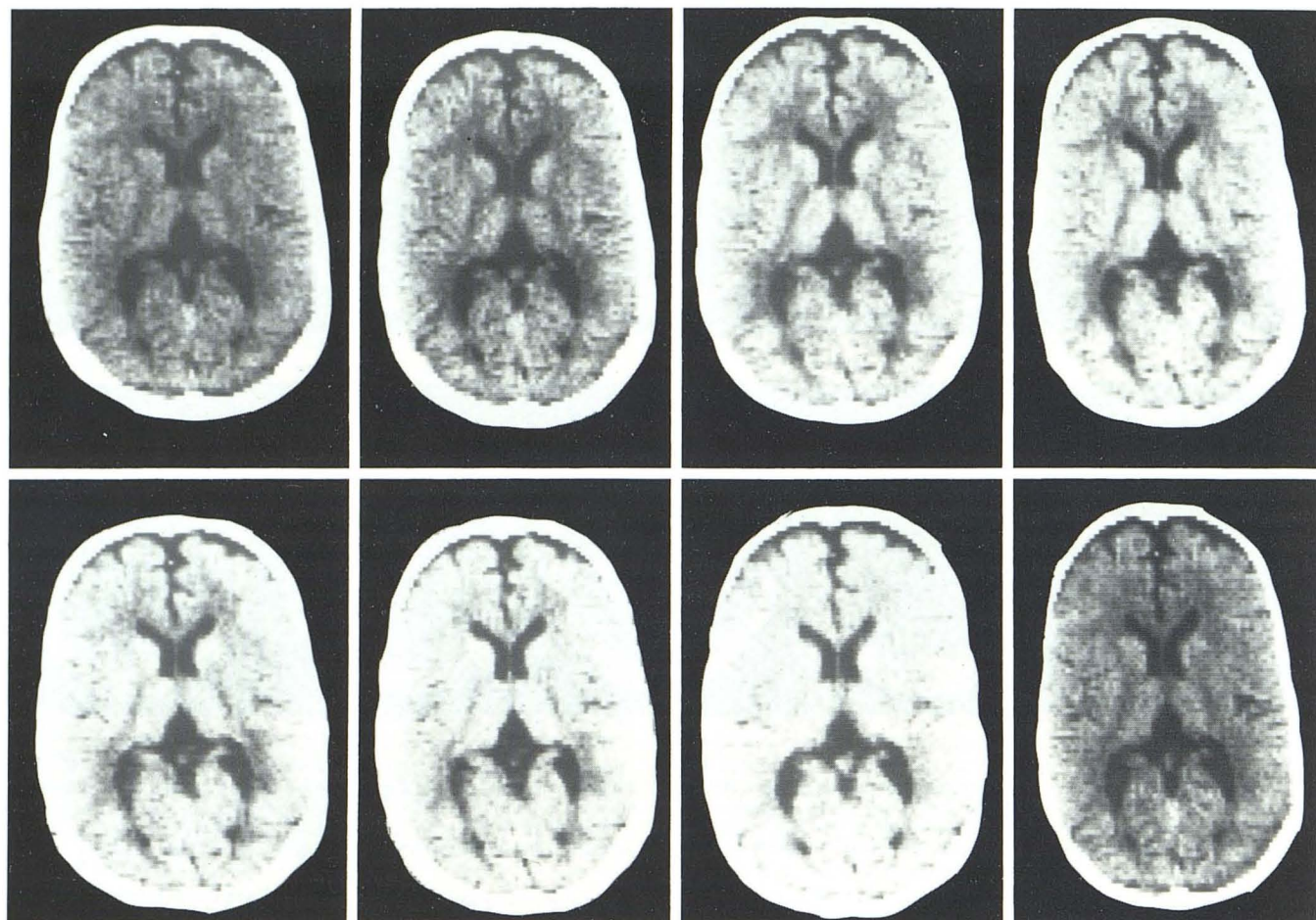
Fig. 3.—Normal CT with 42% xenon inhalation in patient with sickle cell disease and seizures but without focal neurologic deficit. *Top, left to right*: baseline scan before xenon inhalation; at 1 min 45 sec; 2 min 55 sec; and 4 min 5 sec after onset of inhalation. Gray matter enhances more rapidly than white matter. *Bottom, left to right*: at 5 min 35 sec; 7 min 30 sec; 9 min 55 sec; and baseline (for comparison). Gray matter has achieved equilibrium while white matter continues to show enhancement, consistent with its higher brain-blood partition coefficient (λ).
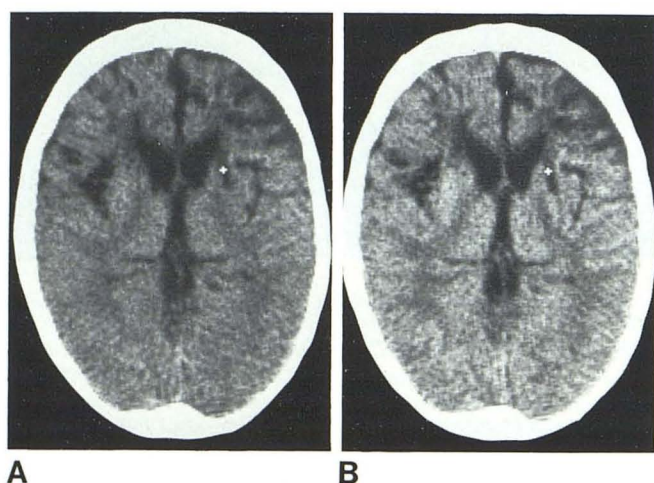

Fig. 4.—Abnormal CT with 45% xenon inhalation in patient with sickle cell disease and multiple small cerebral infarctions. **A**, Baseline scan before xenon inhalation. **B**, At 2 min 55 sec after onset of inhalation. Areas of infarction remain unenhanced and are thus better delineated in **B**.

plasm from vasogenic edema or radiation necrosis. The λ was normal in contralateral brain structures; decreased in the area of vasogenic edema; and increased ($\lambda = 1.24$) in the thalamic region, which contained neoplasm. The λ estimate in this subject was less accurate than in teh other studies since only 5.5 min of the inhalation was monitored in a pathologic process that would have required much longer to equilibrate.

Discussion

Additional diagnostic and functional information was obtained by analyzing the xenon-enhanced CT scans in terms of the general enhancement pattern and increases in CT number over time, even when an absolute value for regional cerebral blood flow was not determined. The calculated brain-blood partition coefficient (λ) of xenon can be used to safely characterize brain tissue in man with a high degree of anatomic specificity.

Abnormalities in both regional cerebral blood flow and λ in cerebral infarction have previously been defined in xenon CT studies [3, 5]. The ability to independently calculate λ is a major advantage of the CT technique as compared with xenon radionuclide studies. Preferential enhancement of normal brain as compared with devitalized brain improves the visualization of subtle or

Fig. 5.—Abnormal CT with 33% xenon inhalation in patient with glioblastoma multiforme and vasogenic edema. *Top, left to right*: baseline scan before xenon inhalation; at 50 sec; at 1 min 45 sec. *Bottom, left to right*: at 3 min 30 sec; 4 min 30 sec; and 5 min 30 sec after onset of inhalation. Gradually increasing enhancement in gray-matter structures contralateral to tumor. Involved thalamus (*open arrows*) enhances more slowly but to a greater degree ($\lambda = 1.24$) than contralateral thalamus. Vasogenic edema (*arrowheads*) enhances more slowly and has lower partition coefficient ($\lambda = 0.72$) than normal white matter ($\lambda = 1.38$).
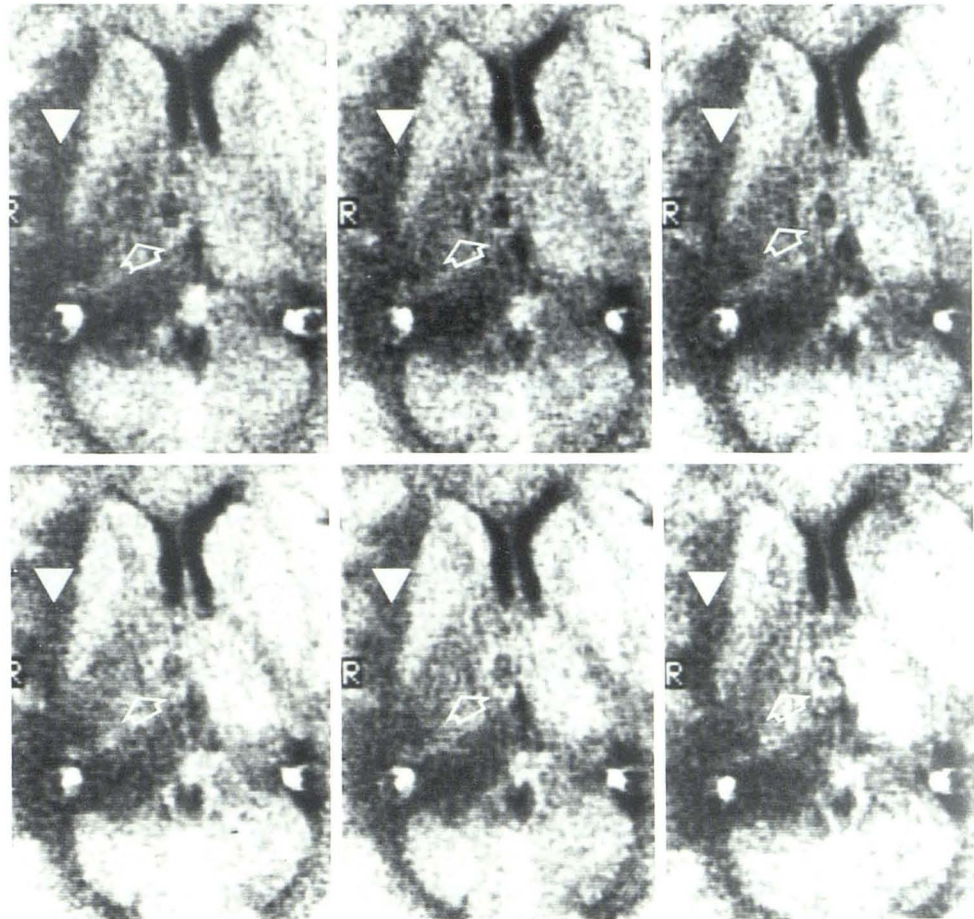
small infarctions. Xenon-enhanced scanning thus improves lesion detection even if regional cerebral blood flow is not measured.

The tissue immediately adjacent to the intracerebral hematoma achieved an equilibrium concentration of xenon more rapidly than other brain areas and therefore had a comparatively greater blood flow. This finding of relative hyperperfusion adjacent to an intracerebral hematoma was recently described in an experimental animal model [9]. No other in vivo technique provides the spatial resolution to define an abnormality in flow in such an anatomically specific region.

Even with a diffuse and symmetric abnormality, as in our case of diffuse hypoxic encephalopathy [10], the xenon-enhanced study provided useful information about brain function. If, as in this case, the brain tissue requires a prolonged time to equilibrate while the arterial blood supply equilibrates normally, a decrease in regional cerebral blood flow can be surmised even without obtaining an absolute numerical value. The ultimate distribution of xenon between the blood and the brain compartments as reflected in the λ was nevertheless within the normal range in this patient.

Extreme variability in the λ for xenon is well documented for neoplasms involving the central nervous system [11, 12]. However, if the derived λ is increased in some part of the tumor, the differential diagnostic possibility of infarction becomes quite unlikely. Necrotic, cystic, ischemic, and hyperemic parts of the same neoplasm may explain this variability in calculated λ as well as in regional cerebral blood flow. The increased water content of the white matter involved with vasogenic edema might account for decreases in blood flow and λ. A future application of xenon-enhanced CT might involve the distinction between residual glial neoplasms (mildly increased λ and decreased regional flow) and radiation necrosis (decreased λ and severely decreased regional flow).

Xenon-133 blood flow studies [13] and glucose utilization studies using positron emission tomography [14, 15] have mapped brain function in terms of the activation of the visual, auditory, and motor cortex. The same types of studies can be conducted with xenon-enhanced CT, although they are certainly more cumbersome to perform when the subjects are inhaling nonradioactive xenon through a ventilatory apparatus. Advantages of using the xenon CT method are the higher degree of anatomic specificity and the ability to repeat studies at 20 min intervals.

Finally, a number of potential difficulties may arise in using quantitative data about brain activity and λ. These include: (1) lack of patient cooperation and head motion; (2) minor instabilities in the derived CT numbers; (3) resolution versus contrast sacrifice in determining optimal kilovoltage and milliamperage; (4) partial volume averaging effects in selecting regions of interest, with smaller sizes providing greater anatomic specificity while larger sizes offer greater statistical accuracy; (5) lack of homogeneity in gray-matter tissue; and (6) biologic limits to maximum enhancement with nonanesthetic levels of xenon inhalation.

REFERENCES

1. Drayer BP, Gur D, Wolfson SK, Dujovny M. Regional blood flow in the posterior fossa. Xenon enhanced CT scanning. *Acta Neurol Scand [Suppl]* **1979**;60:218–219

2. Drayer BP, Gur D, Wolfson SK, Cook EE. Experimental xenon enhancement with CT imaging: cerebral applications. *AJNR* **1980**;1:3–8, *AJR* **1980**;134:39–44

3. Drayer BP, Gur D, Yonas H, Wolfson SK, Cook EE. Abnormality of the xenon brain-blood partition coefficient and blood flow in cerebral infarction. *Radiology* **1980**;135:349–354

4. Meyer JS, Hayman LA, Yamomoto M, et al. Local cerebral blood flow measured by CT after stable xenon inhalation. *AJNR* **1980**;1:213–225

5. Meyer JS, Heyman A, Amano T, et al. Mapping local blood flow of human brain by CT scanning during xenon inhalation. *Stroke* **1981**;12:426–436

6. Kelcz F, Hilal SK, Hartwell P, Joseph PM. Computed tomographic measurement of xenon brain-blood partition coefficient and implications for regional cerebral blood flow: a preliminary report. *Radiology* **1978**;127:385–392

7. Drayer BP. Functional applications of CT of the central nervous system. *AJNR* **1981**;2:495–510

8. Obrist W, Thompson HK, Wang HS, Wilkinson WE. Regional cerebral blood flow estimated by [133]xenon inhalation. *Stroke* **1975**;6:245–256

9. Ropper AH, Zervas NT. Cerebral blood flow after experimental basal ganglia hemorrhage. *Ann Neurol* **1982**;11:266–271

10. Ingvar DH, Haggendal E, Nilsson NH. Cerebral circulation and metabolism in a comatose patient. *Arch Neurol* **1964**;11:13–21

11. O'Brien MD, Veall N. Partition coefficients between various brain tumors and blood for [133]Xe. *Phys Med Biol* **1974**;19:472–475

12. Radue EW, Kendall BE. Xenon enhancement in tumors and infarcts. *Neuroradiology* **1978**;16:224–227

13. Ingvar DH, Lassen NA. Cerebral function, metabolism, and blood flow. *Acta Neurol Scand* **1978**;57:262–269

14. Phelps ME, Mazziotta JC, Kuhl DE, et al. Tomographic mapping of human cerebral metabolism. Visual stimulation and deprivation. *Neurology* (NY) **1981**;31:517–529

15. Mazziotta JC, Phelps ME, Carson RE, Kuhl DE. Tomographic mapping of human cerebral metabolism: auditory stimulation. *Neurology* (NY) **1982**;32:921–937